Inositol Hexakisphosphate Is Bound in the ADAR2 Core and Required for RNA Editing

Mark R. Macbeth,[1,2] Heidi L. Schubert,[1] Andrew P. VanDemark,[1] Arunth T. Lingam,[1,2] Christopher P. Hill,[1]* Brenda L. Bass[1,2]*

We report the crystal structure of the catalytic domain of human ADAR2, an RNA editing enzyme, at 1.7 angstrom resolution. The structure reveals a zinc ion in the active site and suggests how the substrate adenosine is recognized. Unexpectedly, inositol hexakisphosphate (IP_6) is buried within the enzyme core, contributing to the protein fold. Although there are no reports that adenosine deaminases that act on RNA (ADARs) require a cofactor, we show that IP_6 is required for activity. Amino acids that coordinate IP_6 in the crystal structure are conserved in some adenosine deaminases that act on transfer RNA (tRNA) (ADATs), related enzymes that edit tRNA. Indeed, IP_6 is also essential for in vivo and in vitro deamination of adenosine 37 of $tRNA^{ala}$ by ADAT1.

One form of RNA editing is catalyzed by adenosine deaminases that act on RNA (ADARs), a family of enzymes that deaminate adenosine to form inosine in double-stranded RNA (dsRNA) (Fig. 1A) (*1*). ADARs are important for proper neuronal function (*2*–*4*) and also are implicated in the regulation of RNA interference (RNAi) (*5*–*7*). Inosine is recognized as guanosine by most cellular proteins and the translation machinery, and it pairs most stably with cytidine. Therefore, editing of RNA can alter a codon, create splice sites, and change its structure. The latter occurs when an AU base pair is changed to an IU mismatch and may be important for the effects of ADARs on the RNAi pathway.

ADARs from all organisms have a common domain structure consisting of one to three dsRNA binding motifs (dsRBMs) near the N terminus, followed by a conserved C-terminal catalytic domain (*1*, *8*). Human ADAR2 (hADAR2) contains two dsRBMs, and its best characterized substrates are the pre-mRNAs of glutamate and serotonin receptors (*9*, *10*). Editing of codons within these RNAs leads to altered amino acids and generates receptors with altered function. hADAR2 also edits its own message to create a new splice site (*11*). Purified hADAR2 deaminates substrates in vitro (*12*) in the absence of any added cofactors, and deletions of N-terminal sequences, including dsRBM1, result in an active protein that accurately edits an RNA substrate (*13*). In addition, we found that a protein consisting of only the catalytic deaminase domain of hADAR2 (hADAR2-D, residues 299 to 701) (fig. S1A) was active in vitro, although it deaminates RNA less efficiently than full-length hADAR2 (fig. S1B).

The structure of the ADAR2 catalytic domain. To better understand the ADAR mechanism, we crystallized hADAR2-D. The structure (PDB code 1ZY7) was determined by multiple isomorphous replacement and refined at 1.7 Å resolution to an R_{factor} of 17.4% and R_{free} of 20.7% (*14*). The asymmetric unit includes 669 water molecules, one sulfate ion, and two hADAR2-D molecules that are essentially identical [root mean square deviation (RMSD) = 0.28 Å for 358 pairs of Cα atoms]. The refined hADAR2-D model contains residues 306 to 461 and 474 to 700 (462 to 473 are disordered), one zinc ion, and one molecule of inositol hexakisphosphate (IP_6).

The protein adopts a roughly spherical 40 Å diameter structure (Fig. 1B) that, consistent with sizing chromatography of hADAR2-D and equilibrium ultracentrifugation of the full-length hADAR2, appears monomeric in the crystal. The active site is indicated by an ordered zinc ion that coordinates a water molecule that presumably displaces ammonia during the deamination reaction. Coordination of the zinc ion by H394, C451, and C516, and hydrogen bonding of the water molecule by E396 (Fig. 1C), is

[1]Department of Biochemistry and [2]Howard Hughes Medical Institute, University of Utah, Salt Lake City, UT 84132, USA.

*To whom correspondence should be addressed. E-mail: bbass@howard.genetics.utah.edu (B.L.B.); chris@biochem.utah.edu (C.P.H.)

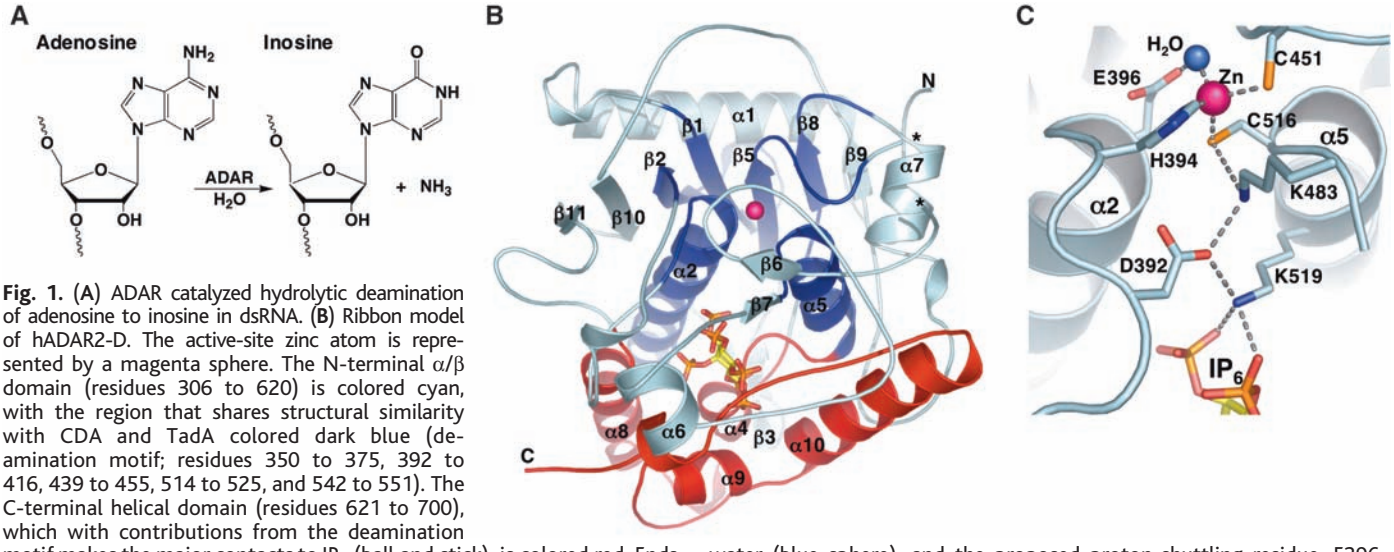

Fig. 1. (**A**) ADAR catalyzed hydrolytic deamination of adenosine to inosine in dsRNA. (**B**) Ribbon model of hADAR2-D. The active-site zinc atom is represented by a magenta sphere. The N-terminal α/β domain (residues 306 to 620) is colored cyan, with the region that shares structural similarity with CDA and TadA colored dark blue (deamination motif; residues 350 to 375, 392 to 416, 439 to 455, 514 to 525, and 542 to 551). The C-terminal helical domain (residues 621 to 700), which with contributions from the deamination motif makes the major contacts to IP_6 (ball and stick), is colored red. Ends of the disordered segment (residues 462 to 473) are indicated with asterisks. (**C**) Residue interactions at the active site. Shown are the zinc ion, coordinating residues (H394, C451, and C516), the nucleophilic water (blue sphere), and the proposed proton-shuttling residue, E396. The hydrogen-bond relay that connects the active site to the IP_6 is also indicated. Single-letter abbreviations for amino acid residues are defined in (*42*).

essentially identical to the geometry seen at the catalytic centers of cytidine deaminase (CDA) (*15*) and TadA (*16*), a member of the ADAT2 (adenosine deaminase that acts on tRNA 2) family. This similarity was predicted earlier on the basis of equivalent chemistry and sequence conservation of the four residues that coordinate zinc and water (*17*, *18*).

Superposition of zinc, water, and coordinating residues was used as the starting point to identify residues of hADAR2-D that were structurally equivalent to those in CDA and TadA (PDB codes 1CTU and 1WWR, respectively). Inspection shows that 77 residues (RMSD = 3.05 Å on Cα atoms) form a structurally conserved "deamination motif" comprising two helices (α2 and α5), four strands (β1, β2, β5, and β8), and connecting loops (Fig. 1B, dark blue). Other hADAR2-D residues do not have structural equivalents in CDA and TadA (Fig. 2A). Further emphasizing the large evolutionary separation between these enzymes, only four of the deamination motif residues have conserved identities in all three enzymes (excluding zinc/water ligands).

The active site of ADAR2. The site of nucleophilic attack during the ADAR reaction (C6 of adenine) lies deep in the major groove of the dsRNA substrate. Because this site is inaccessible to an enzyme, ADARs may use a base-flipping mechanism (*19*, *20*) like other enzymes that modify double-stranded polynucleotides (*21*). Consistent with this scenario, the catalytic zinc center is located in a deep pocket in the enzyme surface that is surrounded by positive electrostatic potential that likely serves as the dsRNA binding site (Fig. 2B). In contrast, TadA uses an alternative mechanism of substrate selection that probably involves recognition of the anticodon stem/loop of tRNA (*16*).

To model binding of substrate, we overlapped the structure of a CDA-zebularine (cytidine analog inhibitor) complex (*15*) onto the hADAR2 structure and built the adenosine monophosphate (AMP) portion of an ADAR substrate to maintain the same catalytic geometry. In this simple overlap based on zinc ion and coordinating residues, the zebularine ribose clashes with the hADAR2 loop containing T375 (Fig. 2C), thereby providing a plausible explanation for why ADARs do not deaminate cytidine. The steric clash is absent with AMP because of the additional distance afforded by the purine ring (Fig. 2D). The proposed AMP-binding geometry requires repositioning of the hADAR2 R455 side chain, although this could be accomplished through minor rearrangements that may occur upon dsRNA binding.

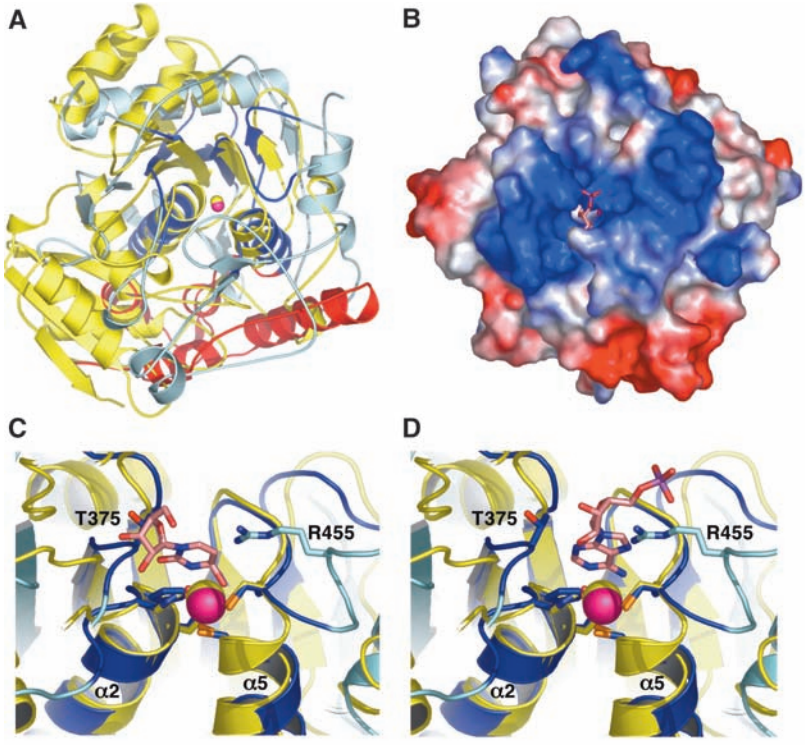

Fig. 2. (**A**) Superposition of *Escherichia coli* CDA (yellow) and hADAR2-D (color scheme as in Fig. 1B) shows that these structures are highly diverged. View direction is similar to Fig. 1B. The only hADAR2-D residues that have structural equivalents in CDA are dark blue. (**B**) Electrostatic surface potential reveals a highly basic (blue) region flanking the active site. View direction is from the top of (A). The modeled AMP (pink) and catalytic zinc ion (magenta, partially occluded) are visible in the active site cleft. (**C**) Superposition of the hADAR2 and CDA active sites. Zebularine (pink) bound to CDA would clash with the loop containing T375 of hADAR2-D. (**D**) Docking of AMP (pink) in the same chemically equivalent orientation as zebularine would not clash with the T375 loop. Single-letter abbreviations for amino acid residues are defined in (*42*).

Comparison of the ADAR and CDA/TadA structures reveals an important difference in the arrangement of the two cysteine residues that coordinate zinc (fig. S5). As often found in zinc-dependent enzymes (*22*, *23*), the two cysteines of CDA and TadA are located in a Cys-X-X-Cys motif at the N terminus of a helix. The first cysteine forms hydrogen bonds with two main-chain amide NH groups at the helix terminus; this likely contributes to catalysis by increasing the positive character of the zinc ion and nucleophilicity of the water molecule (*24*). In ADAR2, however, C451 and C516 are separated by a 64-residue loop, and hydrogen bonding to main-chain atoms is reduced to a single bond between C451 and the amide NH group of C516. However, a second hydrogen bond is observed between C516 and K483 (Fig. 3A and fig. S5), and thus ADARs may have evolved a compensating interaction; K483 is conserved in ADAR sequences but not seen in CDA or TadA.

Inositol hexakisphosphate binds in the core of the catalytic domain. One side of the deamination motif of hADAR2 contributes to a cavity, not found in CDA or TadA, that is formed mainly by C-terminal elements (Fig. 1B, red) and buries the IP_6 molecule and 29 associated water molecules. The identity of IP_6 was suggested by the strong, distinctive electron density (Fig. 3A and fig. S3) and the local electrostatic interactions, and was confirmed by (+) ion electrospray mass spectrometry [observed molecular weight (MW) of IP_6 in complex with the protein = 660.0 Da; calculated MW = 659.9 Da] (*14*). IP_6 is an abundant inositol polyphosphate implicated in many cellular functions, including RNA export, DNA repair, endocytosis, and chromatin remodeling (*25*–*29*). Intriguingly, the compound is reported to affect neuronal AMPA receptors (*30*), whose messages are edited by ADAR2 (*9*).

The IP_6 cavity is extremely basic and lined with many arginine and lysine residues (R400, R401, and R522 and K519, K629, K662, K672, and K690), as well as W523, W687, Y658, and Y668 (Fig. 3, A and B). Most of these residues are invariant among catalytically active ADARs, as well as in the ADAT1 family of enzymes, which deaminate A37 of certain tRNAs. (The ADAT2 family, of which TadA is a member, is distinct from ADAT1 and does not have the IP_6 binding pocket or its conserved residues.)

IP_6 was not added during purification or crystallization but must have been acquired during expression of the human ADAR2-D protein in *Saccharomyces cerevisiae*, which like other eukaryotes has pools of IP_6 (*31*). The presence of IP_6 in the purified protein therefore indicates a tight association, consistent with the extensive array of hydrogen bonds formed with conserved side chains (Fig. 3B) and the almost completely buried environment (Fig. 3C). The structure suggests that hADAR2 will be nonfunctional in the absence of IP_6, a view that is supported by experiments described below.

IP_6 is required for ADAR2 activity. In *S. cerevisiae*, the last step in the synthesis of IP_6 is the phosphorylation of IP_5 by Ipk1p, and yeast harboring a deletion of *IPK1* are viable but fail to produce IP_6 (*25*). To test for the IP_6 requirement of hADAR2, we expressed the protein in *ipk1*Δ yeast cells and compared its activity to hADAR2 expressed in the same strain but containing the *IPK1* gene. As substrate, we used a 27-base-pair RNA that mimics the natural arginine/glycine (R/G) editing site of the glutamate receptor B (gluR-B) pre-mRNA (Fig. 4A) and that is efficiently edited by hADAR2 in vitro (*20*). IP_6 was required for hADAR2 activity (Fig. 4B), because there was no editing of this RNA by protein expressed in the *ipk1*Δ mutant. Using reverse transcription polymerase chain reaction (RT-PCR), we determined that hADAR2 mRNA was expressed at the same levels in the wild-type and *ipk1*Δ mutant strains, although the amount of hADAR2 protein was lower by a factor of 5 to 10 in the mutant strain. Western blots were performed to determine the amount of hADAR2 protein in each extract by comparison with a standard curve generated with known amounts of purified, histidine-tagged protein (R_2D, an N-terminal truncation of hADAR2) (*13*). This information was used to normalize amounts of hADAR2 used for the in vitro assays, and a Western blot confirmed that amounts of hADAR2 in wild-type and mutant editing reactions were similar (Fig. 4C).

IP_6 is required for tRNA editing by the ADAT1 family of deaminases. ADATs are another class of enzymes that deaminate adenosine to generate inosine in RNA. These enzymes contain only the catalytic domain and deaminate tRNAs at adenosines 34 and 37 (A34 and A37) (*18*). On the basis of their sequences and substrates, there are three types of ADATs in eukaryotes. ADAT1 deaminates A37 of $tRNA^{ala}$ (*32*), and the resulting inosine is subsequently methylated at N1 in a reaction requiring a different enzyme and S-adenosylmethionine (*33*). ADAT2 and ADAT3 form a heterodimer that deaminates A34 of various tRNAs and, consistent with the fact that this is the wobble position, unlike ADAT1, these enzymes are essential (*32*, *34*). By aligning enzyme sequences, we noted that residues observed to coordinate IP_6 in the hADAR2 crystal structure were conserved in the ADAT1 family but not in the ADAT2 or ADAT3 families (Fig. 5A and fig. S6). To test the consequent prediction that ADAT1, but not ADAT2/3, requires IP_6, we monitored activity of endogenous ADAT in extracts prepared from *S. cerevisiae* wild-type or *ipk1*Δ strains. *S. cerevisiae* $tRNA^{ala}$ is deaminated at A34, as well as A37, and provided an ideal substrate with which to assay the IP_6 requirement of the different ADATs (Fig. 5B). We observed that in vitro editing of A37 by ADAT1 is severely reduced in extract prepared from the *ipk1*Δ strain compared with extract from a wild-type strain (Fig. 6A). In contrast, there was no difference for in vitro editing of A34 by the ADAT2/ADAT3 heterodimer in the mutant versus the wild-type extract (Fig. 6B). To confirm that the lack of activity in the *ipk1*Δ strain derived from a lack of IP_6 rather than a molecule downstream in the pathway, we tested ADAT1 activity in extracts prepared from a *kcs1*Δ mutant (fig. S7). The *KCS1* gene product is downstream of *IPK1* in the inositol polyphosphate synthesis pathway and phosphorylates IP_6 to form the pyrophosphate-containing IP_7 (5PP-IP_5) (*35*). The *kcs1*Δ mutation had no effect on the A37 editing activity of ADAT1, which indicates that the editing defect in the *ipk1*Δ mutant is due to the IP_6 deficiency.

The existence of the *ipk1*Δ mutant, and the fact that *S. cerevisiae* $tRNA^{ala}$ is deaminated at both A34 and A37, provided a facile system for analyzing the in vivo requirement for IP_6. RNA was prepared from wild-type or *ipk1*Δ cells, $tRNA^{ala}$ was amplified using RT-PCR, and the RT-PCR product was sequenced (Fig. 6C). Because inosine is read as guanosine by reverse transcriptase, edited adenosines were identified as guanosine in the dideoxy sequencing reaction. Consistent with the in vitro data, we observed that A34 is edited with equal efficiency in the wild-type and mutant strain, but A37 is edited

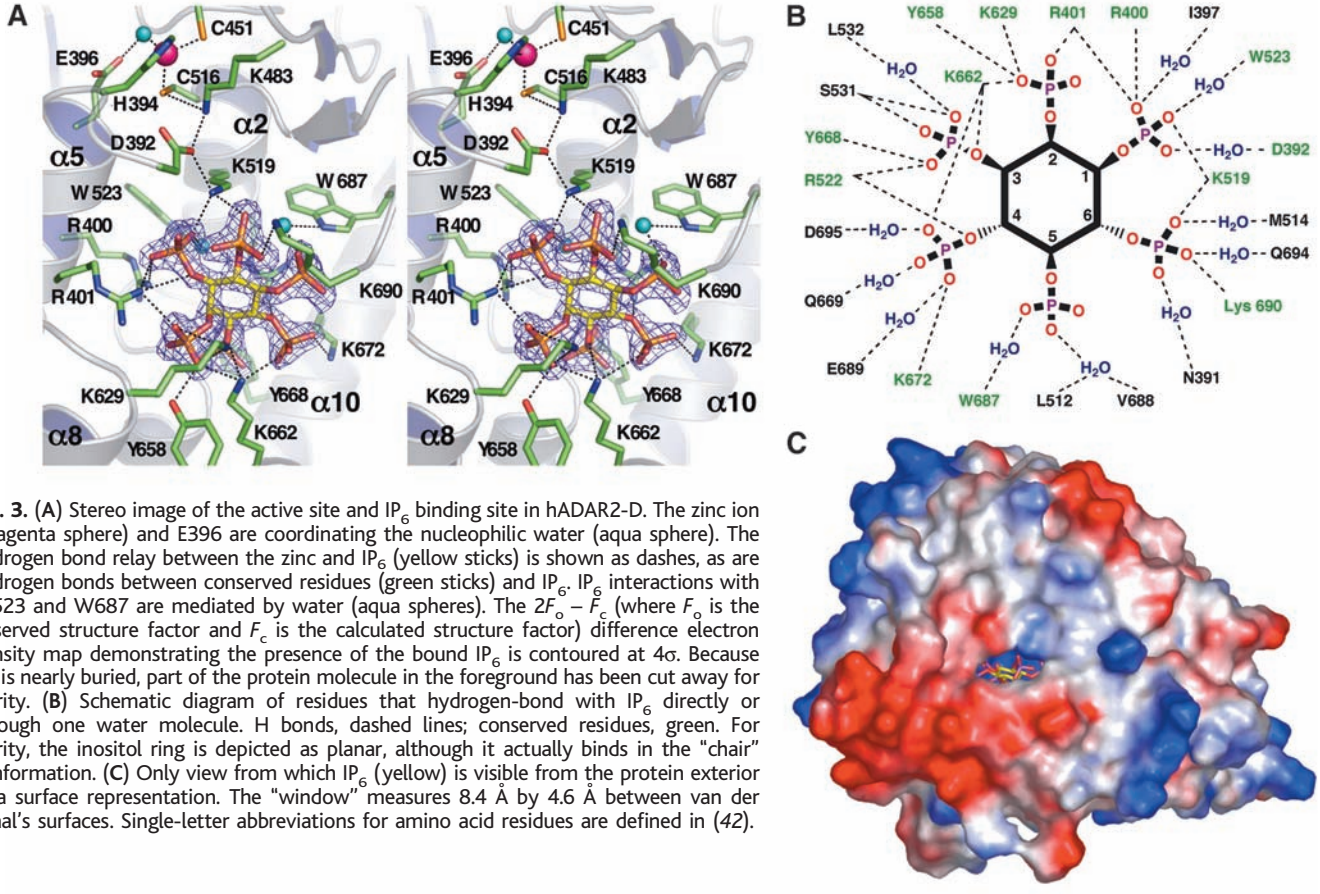

Fig. 3. (**A**) Stereo image of the active site and IP_6 binding site in hADAR2-D. The zinc ion (magenta sphere) and E396 are coordinating the nucleophilic water (aqua sphere). The hydrogen bond relay between the zinc and IP_6 (yellow sticks) is shown as dashes, as are hydrogen bonds between conserved residues (green sticks) and IP_6. IP_6 interactions with W523 and W687 are mediated by water (aqua spheres). The $2F_o - F_c$ (where F_o is the observed structure factor and F_c is the calculated structure factor) difference electron density map demonstrating the presence of the bound IP_6 is contoured at 4σ. Because IP_6 is nearly buried, part of the protein molecule in the foreground has been cut away for clarity. (**B**) Schematic diagram of residues that hydrogen-bond with IP_6 directly or through one water molecule. H bonds, dashed lines; conserved residues, green. For clarity, the inositol ring is depicted as planar, although it actually binds in the "chair" conformation. (**C**) Only view from which IP_6 (yellow) is visible from the protein exterior in a surface representation. The "window" measures 8.4 Å by 4.6 Å between van der Waal's surfaces. Single-letter abbreviations for amino acid residues are defined in (*42*).

much less efficiently in the *ipk1*Δ strain (Fig. 6C). A37 in the wild-type strain is read as a thymidine, presumably due to N^1-methylinosine at position 37. m^1I, like m^1A, may pair with reduced specificity in the reverse transcription reaction, explaining the presence of a T in the PCR product (*36*).

In the crystal structure of hADAR2, IP_6 binds and fills an extremely basic hole, with the center of the inositol ring more than 10 Å from the protein surface. Thus, it seems possible that ADAR2 and, by analogy, ADAT1, are unstable without IP_6. In this regard we wondered about the nature of ADAT1 expressed in the *ipk1*Δ mutant. Was this protein trapped in an irreversible inactive state or forming a folding intermediate that could bind IP_6 to achieve its active conformation? To explore this question, we tested whether the addition of IP_6 to extracts prepared from the *ipk1*Δ mutant could recover ADAT1 activity. When added to extracts prepared from the *ipk1*Δ strain, IP_6 recovered activity to ~50% of wild-type (Fig. 7, A and C), which suggests that the protein does not require IP_6 during its synthesis and the initial stages of folding. As expected, the addition of IP_6 to wild-type extract had no effect, because these cells are capable of synthesizing IP_6 (Fig. 7, B and C). To test for the specific requirement for IP_6 by ADAT1, we performed a similar experiment, except we substituted inositol hexakissulfate (IS_6) for IP_6. Despite its similar charge and structure, IS_6 does not recover ADAT1 activity when added to *ipk1*Δ extracts (Fig. 7A). This suggests that the enzyme specifically requires IP_6 for function and can discriminate between the minor differences in phosphate/sulfate chemistry (e.g., the protonation state).

So far, we have been unable to rescue the activity of hADAR2 expressed in the *ipk1*Δ by adding IP_6. Possibly, native *S. cerevisiae* ADAT1, but not the heterologous hADAR2, is associated with a host chaperone in the extract that promotes refolding in the presence of IP_6. Alternatively, this result may hint at interesting differences between the two enzymes in IP_6 accessibility. Such a difference might explain why assays of ADAT1 in *ipk1*Δ extracts show a small (~5%) amount of A37 deamination at the highest concentrations of extract (Fig. 6A), whereas ADAR2 expressed in this strain shows no residual activity. If the IP_6 binding site in ADAT1 were more accessible than that of ADAR2, it might bind a noncognate inositol polyphosphate, such as IP_5, to allow a low level of activity.

Discussion. Burial of IP_6 may reflect a novel way of using an available cellular component to define and stabilize a protein fold. This would be analogous to the use of "structural" metal ions in stabilizing the fold of metalloproteins. To our knowledge, this represents the first example of a protein using IP_6 for this purpose. Other protein structures with bound IP_6 have been reported, such as deoxyhemoglobin (*37*) and the clathrin adaptor complex AP2 (*38*); however, unlike ADAR2-D, in these cases the IP_6 molecule is not extensively buried and does not appear to dramatically stabilize the overall structure.

In addition to the structural requirement, IP_6 may play a subtle role in modulating catalytic efficiency by indirectly ordering the side chain of K483. Two of the IP_6 phosphate groups approach within 10 Å of the catalytic zinc ion and are indirectly coordinated to zinc by a chain of hydrogen-bonded residues that includes K519, D392, and K483 (Fig. 3A). These residues are conserved among active ADARs, and K483 may contribute to tuning the pK_a of the nucleophilic water molecule through its interaction with C516 (Fig. 3A).

Sequence alignments indicate that ADAT1 enzymes are the evolutionary link between the other family members, ADAT2/3 (including TadA) and ADARs (*18*). ADAT1 apparently

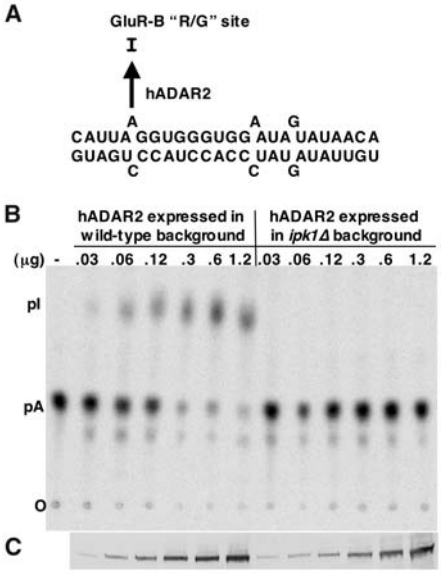

Fig. 4. (**A**) The 27-mer R/G site RNA substrate used to assay hADAR2 editing activity. (**B**) Editing of the R/G site RNA by hADAR2 expressed in wild-type or *ipk1*Δ yeast. The R/G site adenosine was labeled with ^{32}P and incubated with increasing concentrations of expressed hADAR2 in extracts. Reacted RNA was treated with nuclease P1, the resulting 5′ nucleotide monophosphates separated by thin-layer chromatography (TLC), and the plate exposed to a PhosphorImager screen. The amount of hADAR2 in each extract was determined by Western blotting, and extract was added to give the final ADAR2 concentrations as indicated. (**C**) Western blot showing the amount of hADAR2 in each reaction. Single-letter abbreviations for amino acid residues are defined in (*42*).

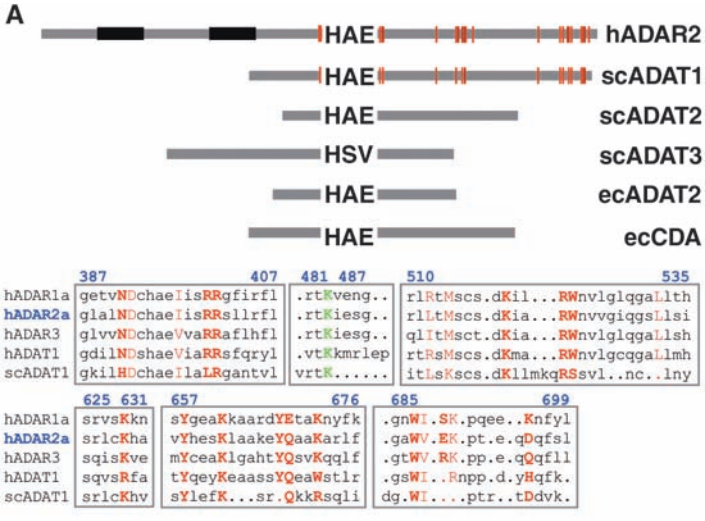

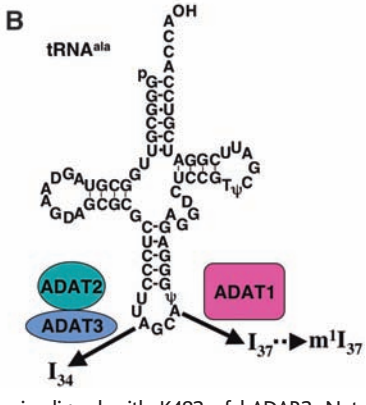

Fig. 5. (**A**) Schematic diagram showing the relative lengths and domain structures of hADAR2 and family members from *S. cerevisiae* (sc) and *E. coli* (ec). Proteins are anchored at the invariant zinc-coordinating histidine (H). Residues that coordinate IP_6 are red lines; double-stranded RNA binding motifs are in black. Alignments for regions surrounding the residues that coordinate IP_6 in hADAR2 are shown below, with blue numbering corresponding to hADAR2. IP_6 coordinating residues are in red, with side-chain contacts in bold. Residues N391, W523, Q669, W687, E689, and D695 are water-mediated contacts. The conserved K483, which is part of a hydrogen-bond relay from IP_6 to the active site zinc, is shown in green. Sequences diverge considerably in the region surrounding K483; the alignment shown was chosen because the conserved lysine of various subfamilies is aligned with K483 of hADAR2. Notably, the IP_6 coordinating residues are found in ADAR3, which suggests that inefficient IP_6 binding is not the reason this enzyme lacks deaminase activity (*43*). (**B**) The $tRNA^{ala}$ substrate used in this study showing the sites of modification by the ADAT proteins. Single-letter abbreviations for amino acid residues are defined in (*42*).

Fig. 6. (**A**) Editing of tRNA^{ala} A37 in vitro by extracts of wild-type or *ipk1*Δ yeast strains. tRNA^{ala}, labeled with ^{32}P at A37, was incubated with increasing amounts of yeast extract protein, as indicated (*14*). Reacted RNA was processed as in Fig. 4B, and nuclease P1 products were separated by TLC (left). The fraction of inosine in each lane was quantified, and the average of three determinations was plotted as a function of protein concentration (right; error bars, standard deviation; when error was very small, error bars are obscured by data point symbols). Solid line, editing by ADAT1 from wild-type extracts; dashed line, editing by ADAT1 from *ipk1*Δ extracts. (**B**) As in (A) but showing editing of A34-labeled tRNA^{ala}. Solid line, editing by ADAT2/3 from wild-type extracts; dashed line, editing by ADAT2/3 from *ipk1*Δ extracts. (**C**) Editing of endogenous tRNA in vivo. tRNA was prepared from wild-type or *ipk1*Δ strains, reverse transcribed, and amplified by PCR. PCR products were sequenced using dideoxy nucleotide triphosphates and a ^{32}P-labeled primer that anneals to the nontemplate strand at the 5′ end of the gene. The right panel shows an expanded view of the sequencing gel shown on the left. The dideoxy sequencing lanes are indicated at the top of each lane, and the 5′ to 3′ sequence to the left of the gel is read from bottom to top. Bands corresponding to A34 to G editing in the wild-type and *ipk1*Δ tRNAs are labeled with daggers, and the band representing the A37 site that is not edited in the *ipk1*Δ tRNA is labeled with an asterisk. Consistent with the observation of residual activity in the mutant extract in vitro (A), some editing of A37 in the mutant extract occurs.

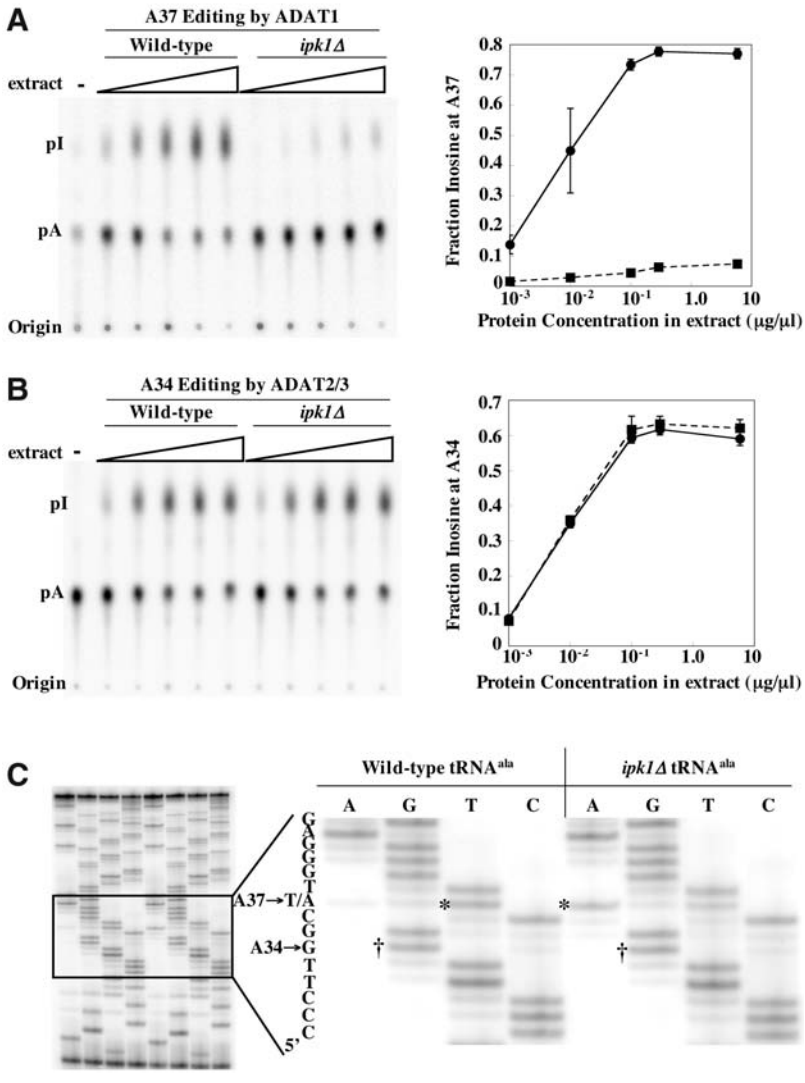

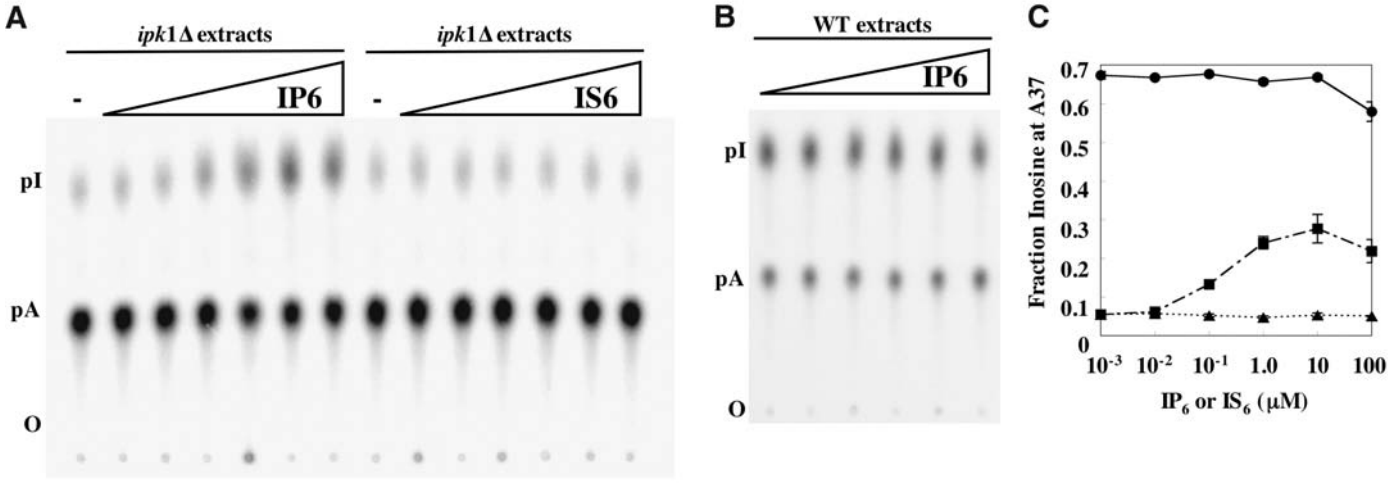

Fig. 7. (**A**) Addition of IP$_6$, but not IS$_6$, rescued ADAT1 activity in extracts prepared from *ipk1*Δ yeast. Wild-type or *ipk1*Δ protein extract (0.1 μg/μl) was incubated with IP$_6$ or IS$_6$ for 15 min at 30°C before the addition of A37-labeled tRNA^{ala}. IP$_6$ and IS$_6$ concentrations were 10-fold dilutions from 100 μM to 10^{-3} μM. The tRNA was processed as described in Fig. 4B. (**B**) Addition of IP$_6$ had no effect on ADAT1 activity in wild-type extracts using the reaction conditions of (A). Without the addition of IP$_6$, wild-type extracts gave 70% A to I conversion. (**C**) The average fraction of inosine produced in three experiments each of (A) and (B) plotted as a function of IP$_6$ or IS$_6$ concentration; error bars show the standard deviation (small error bars are obscured by the data point symbol). Circles, ADAT1 activity from wild-type extracts with IP$_6$ added; squares, activity of *ipk1*Δ extracts with IP$_6$; triangles, activity of *ipk1*Δ extracts with IS$_6$.

diverged from the ADAT2/3 family by acquiring the ability to bind IP_6, followed by the acquisition of one or more dsRBMs to generate an ADAR. ADAT1 may have evolved an IP_6 binding function as a means of regulation. IP_6 accumulates in yeast during times of stress (*39*) and thus could lead to increased ADAT1 activity, and consequently to an increased conversion of A37 to N^1-methylinosine. Modification of position 37 is predicted to increase fidelity of protein synthesis by stabilizing the codon-anticodon interaction (*40*), and thus yeast may use this modification to fine-tune protein synthesis in response to environmental conditions.

Once established as a means of regulation for ADAT1, metazoa may have extended this regulatory mode for use in ADARs, which perform important roles in the nervous system and display changes in activity during development (*41*). For example, a feedback mechanism could act through phospholipase C in response to hormones such as serotonin. Upon binding of serotonin to its $5\text{-}HT_{2c}$ receptor, phospholipase C is activated to cleave phosphatidyl inositol 4,5-bisphosphate (PIP_2) to form the second messengers diacylglycerol and inositol 1,4,5-triphosphate (IP_3), which is subsequently phosphorylated to form IP_6. $5\text{-}HT_{2C}$ receptor mRNA is edited at five distinct sites by ADAR2, with the more extensively modified receptors requiring greater concentrations of serotonin to stimulate phospholipase C. It is tempting, therefore, to speculate that the serotonin-induced production of IP_6 causes increased production of active ADAR2, which in turn edits mRNA to attenuate the serotonin signaling pathway.

The structure of the hADAR2 catalytic domain reveals the active site architecture of a zinc-catalyzed deamination reaction and suggests how ADARs discriminate between cytidine and adenosine residues. The presence of IP_6 in the protein core implied an unexpected requirement for this cofactor in ADARs, which was confirmed by assaying the RNA editing activity of enzymes lacking IP_6. The finding that IP_6 is required for ADAR and ADAT activity suggests many interesting links between RNA editing and diverse processes such as cell signaling and translation, thus setting the stage for future studies.

References and Notes

1. B. L. Bass, *Annu. Rev. Biochem.* **71**, 817 (2002).
2. M. Higuchi *et al.*, *Nature* **406**, 78 (2000).
3. M. J. Palladino, L. P. Keegan, M. A. O'Connell, R. A. Reenan, *Cell* **102**, 437 (2000).
4. L. A. Tonkin *et al.*, *EMBO J.* **21**, 6025 (2002).
5. S. W. Knight, B. L. Bass, *Mol. Cell* **10**, 809 (2002).
6. A. D. Scadden, C. W. Smith, *EMBO Rep.* **2**, 1107 (2001).
7. L. A. Tonkin, B. L. Bass, *Science* **302**, 1725 (2003).
8. S. Maas, A. Rich, K. Nishikura, *J. Biol. Chem.* **278**, 1391 (2003).
9. T. Melcher *et al.*, *Nature* **379**, 460 (1996).
10. C. M. Burns *et al.*, *Nature* **387**, 303 (1997).
11. S. M. Rueter, T. R. Dawson, R. B. Emeson, *Nature* **399**, 75 (1999).
12. M. A. O'Connell, A. Gerber, W. Keller, *J. Biol. Chem.* **272**, 473 (1997).
13. M. R. Macbeth, A. T. Lingam, B. L. Bass, *RNA* **10**, 1563 (2004).
14. Materials and methods are available as supporting material on *Science* Online.
15. L. Betts, S. Xiang, S. A. Short, R. Wolfenden, C. W. Carter Jr., *J. Mol. Biol.* **235**, 635 (1994).
16. M. Kuratani *et al.*, *J. Biol. Chem.* **280**, 16002 (2005).
17. U. Kim, Y. Wang, T. Sanford, Y. Zeng, K. Nishikura, *Proc. Natl. Acad. Sci. U.S.A.* **91**, 11457 (1994).
18. A. P. Gerber, W. Keller, *Trends Biochem. Sci.* **26**, 376 (2001).
19. A. G. Polson, B. L. Bass, *EMBO J.* **13**, 5701 (1994).
20. O. M. Stephens, H. Y. Yi-Brunozzi, P. A. Beal, *Biochemistry* **39**, 12243 (2000).
21. X. Cheng, R. J. Roberts, *Nucleic Acids Res.* **29**, 3784 (2001).
22. J. W. Schwabe, A. Klug, *Nat. Struct. Biol.* **1**, 345 (1994).
23. J. E. Wedekind, P. A. Frey, I. Rayment, *Biochemistry* **34**, 11049 (1995).
24. D. C. Carlow, C. W. Carter Jr., N. Mejlhede, J. Neuhard, R. Wolfenden, *Biochemistry* **38**, 12258 (1999).
25. J. D. York, A. R. Odom, R. Murphy, E. B. Ives, S. R. Wente, *Science* **285**, 96 (1999).
26. L. A. Hanakahi, S. C. West, *EMBO J.* **21**, 2038 (2002).
27. M. Hoy *et al.*, *Proc. Natl. Acad. Sci. U.S.A.* **99**, 6773 (2002).
28. X. Shen, H. Xiao, R. Ranallo, W. H. Wu, C. Wu, *Science* **299**, 112 (2003).
29. D. J. Steger, E. S. Haswell, A. L. Miller, S. R. Wente, E. K. O'Shea, *Science* **299**, 114 (2003).
30. B. Valastro *et al.*, *Hippocampus* **11**, 673 (2001).
31. V. Raboy, *Phytochemistry* **64**, 1033 (2003).
32. A. Gerber, H. Grosjean, T. Melcher, W. Keller, *EMBO J.* **17**, 4780 (1998).
33. H. Grosjean *et al.*, *Biochimie* **78**, 488 (1996).
34. A. P. Gerber, W. Keller, *Science* **286**, 1146 (1999).
35. A. Saiardi, J. J. Caffrey, S. H. Snyder, S. B. Shears, *J. Biol. Chem.* **275**, 24686 (2000).
36. M. Kroger, B. Singer, *Biochemistry* **18**, 3493 (1979).
37. A. Arnone, M. F. Perutz, *Nature* **249**, 34 (1974).
38. B. M. Collins, A. J. McCoy, H. M. Kent, P. R. Evans, D. J. Owen, *Cell* **109**, 523 (2002).
39. P. P. Ongusaha, P. J. Hughes, J. Davey, R. H. Mitchell, *Biochem. J.* **335**, 671 (1998).
40. H. Grosjean, C. Houssier, P. Romby, R. Marquet, in *Modification and Editing of RNA*, H. Grosjean, R. Benne, Eds. (ASM Press, Washington, DC, 1998), pp. 113–134.
41. H. Lomeli *et al.*, *Science* **266**, 1709 (1994).

42. Single-letter abbreviations for the amino acid residues are as follows: A, Ala; C, Cys; D, Asp; E, Glu; F, Phe; G, Gly; H, His; I, Ile; K, Lys; L, Leu; M, Met; N, Asn; P, Pro; Q, Gln; R, Arg; S, Ser; T, Thr; V, Val; W, Trp; and Y, Tyr.

43. C. X. Chen *et al.*, *RNA* **6**, 755 (2000).

44. We thank R. Schackmann for synthesis of oligonucleotides and N-terminal sequencing and C. Nelson for mass spectrometry analysis; both are supported by a Cancer Center Support Grant (2P30CA042014). We also thank P. Beal and S. Wente for helpful discussions. This work was supported by grants from the National Institute of General Medical Sciences, GM44073 and GM56775, to B.L.B. and C.P.H., respectively. A.P.V. is supported by a postdoctoral fellowship from the American Cancer Society. B.L.B. is a Howard Hughes Medical Institute Investigator.

Supporting Online Material

www.sciencemag.org/cgi/content/full/309/5740/1534/DC1
Materials and Methods
Figs. S1 to S8
Tables S1 and S2
References

4 April 2005; accepted 29 July 2005
10.1126/science.1113150

REPORTS

Single-Molecule Torsional Pendulum

Jannik C. Meyer,[1]* Matthieu Paillet,[2] Siegmar Roth[1]

We have built a torsional pendulum based on an individual single-walled carbon nanotube, which is used as a torsional spring and mechanical support for the moving part. The moving part can be rotated by an electric field, resulting in large but fully elastic torsional deformations of the nanotube. As a result of the extremely small restoring force associated with the torsional deformation of a single molecule, unusually large oscillations are excited by the thermal energy of the pendulum. By diffraction analysis, we are able to determine the handedness of the molecule in our device. Mechanical devices with molecular-scale components are potential building blocks for nanoelectromechanical systems and may also serve as sensors or actuators.

Carbon nanotubes (*1*, *2*) are likely to be used in future nanoscale devices because of their outstanding mechanical and electrical properties. Nanoelectromechanical devices incorporating multiwalled carbon nanotubes (MWNTs) as motion-enabling elements have been demonstrated; in these devices, the MWNT serves as a torsional spring for small angular deformations (*3*) and torsional oscillations (*4*) or as a bearing for continuous rotational operation (*5*, *6*). Here, we show that it is possible to prepare large moving objects suspended on a single molecule—a single-walled nanotube (SWNT). The cross-section of a SWNT is smaller than that of a MWNT by more than two orders of magnitude, and large deformations are possible within the elastic regime. The moving part returns to its initial position even after being turned by 180°. The ultralow torsional spring constant provided by the

[1]Max Planck Institute for Solid State Research, D-70569 Stuttgart, Germany. [2]Laboratoire des Colloïdes, Verres et Nanomatériaux, Université de Montpellier II, 34095 Montpellier, France.

*To whom correspondence should be addressed. E-mail: j.meyer@fkf.mpg.de

Supporting Material

Materials and Methods

Construction, expression and purification of hADAR2-D

The expression vector encoding hADAR2-D was constructed by PCR amplification from a hADAR2 cDNA template and ligated into the vector YEpTOP2PGAL1 as described previously (*S1*). This construct encodes an N-terminal 10-histidine tag, a TEV protease recognition sequence, and residues 299-701 of hADAR2. The protein was expressed in *S. cerevisiae* and purified using nickel chelating, heparin ion exchange, and gel filtration chromatography, as described for other N-terminal truncations of hADAR2 (*S1*). The purified protein was dialyzed into buffer (20 mM Tris-HCl pH 8.0, 100 mM NaCl, 1 mM 2-mercaptoethanol, and 5% glycerol) and concentrated to 10 mg/ml.

RNA preparation and deamination assays

Duplex RNA encoding sense and antisense sequences of the chloramphenicol acetyl transferase gene (CAT duplex) was internally labeled during *in vitro* transcription with α-^{32}P ATP, and gel purified as previously described (*S2*). The *in vitro* editing assay was performed by incubating purified protein and CAT duplex RNA under conditions described previously (*S1*), with concentrations described in the legend to Figure S1.

Crystallization and Data Collection

hADAR2-D was crystallized by vapor diffusion at 21°C by mixing 2 μl of protein solution with 2 μl of well solution (0.1 M Bis-Tris pH 6.8, 0.2 M $(NH_4)_2SO_4$, 24% PEG 3350, and 7.5% glycerol). After 10 days, crystals were mounted in nylon loops and

cryocooled by plunging into liquid nitrogen. All data were collected at 100 K using a Rigaku R-AXIS IV image plate detector mounted on a rotating anode source. Data were integrated and scaled using the programs DENZO and SCALEPACK (*S3*). The crystals belonged to space group $P2_12_12_1$ and contained two molecules in the asymmetric unit.

Multiple Isomorphous replacement, model building and refinement

Isomorphous heavy atom derivatives were prepared by soaking crystals at room temperature in well solutions containing either 0.5 mM thimerosal ($C_9H_9HgO_2SNa$) or 0.5 mM mercury acetate ($Hg[C_2H_3O_2]_2$) for 1 hour, or 20 mM sodium tungstate (Na_2WO_4) for 3 hours. Data were collected and processed as above, and scaled against the native data set. Heavy atom sites were located by inspection of Patterson functions. Most crystallographic computing used programs from the CCP4 suite (*S4*). Phases from the thimerosal and mercury acetate derivatives were calculated using SOLVE (*S5*), and used to locate two tungstate clusters (each containing the same arrangement of twelve tungsten atoms) in a difference Fourier map (Figure S2). MIR phases from the three derivatives were calculated using SOLVE (figure of merit 0.75) and generated an easily interpretable electron density map after density modification by solvent flattening (42% solvent) using the program RESOLVE (*S6*). An initial model was built by RESOLVE (*S6*), and manually completed using the XFIT program in the XTALVIEW software package (*S7*). The model was refined using REFMAC5 (*S8*), using refinement parameters for the IP_6 ligand that were generated using the SKETCHER program in CCP4 (*S4*). It is possible that some of the solvent molecules currently assigned as water are other species, such as sodium ions, although this is not apparent from the electron density or inspection

of coordination geometry. Figures were generated using the PyMOL molecular graphics system (*S9*) and Figure 3B was initially made using the program LIGPLOT (*S10*) then modified using CHEMDRAW (CambridgeSoft, Cambridge, MA).

Yeast Strains and Extract preparation

hADAR2 was expressed in the strain BCY123 as described previously (*S1*). The *IPK1* gene in this strain was replaced with the kanamycin resistance gene (*ipk1Δ::KanMX*) using a PCR-based gene targeting method (*S11*). The knockout was confirmed by the ability to grow in the presence of the antibiotic G418, and PCR of the genomic DNA. The new strain (BCY123-*ipk1*Δ) was also used to express hADAR2 as described above. Cells were harvested by centrifugation, resuspended in buffer (20 mM Tris-HCl pH 8.0, 100 mM NaCl, 20% glycerol and 1 mM 2-mercaptoethanol) and lysed by three consecutive passes through a French pressure cell at 20,000 psi. The lysate was centrifuged at 100,000 x g for 1 hour at 4°C. The supernatant (S100 extract) was stored in aliquots at -80°C until use in the editing assays.

For the ADAT1 activity assays, the yeast strain BY4743 (wild-type; *S12*) and strains with the same genetic background but having the *IPK1* gene or the *KCS1* gene replaced with *KanMX* (*ipk1Δ::KanMX, kcs1Δ::KanMX)*, were obtained from Research Genetics (Huntsville, AL). The strains were grown in YPD, harvested by centrifugation, and S100 extract was prepared as described above.

RNA preparation

For the in vitro editing assays, RNA substrates were prepared using the splint ligation method of Moore and Sharp (*S13*). The R/G 27-mer RNA used for the hADAR2 editing assays was prepared as described (*S14*). The tRNAs were chemically synthesized in two halves. For labeling A34, the two RNAs spanned residues 1-33 (the 5' half) and 34-76 (the 3' half); for labeling A37, the two RNAs spanned residues 1-36 (the 5' half) and 37-76 (the 3' half). The 3' halves were phosphorylated (at either A34 or A37) with ^{32}P using polynucleotide kinase, and annealed, along with their respective 5' partner, to a DNA "splint" of complementary sequence to the 76-nucleotide tRNA^{ala}. The RNAs were then ligated using T4 DNA ligase, the DNA splint was digested with RQ1 DNase (Promega, Madison, WI), and the RNA purified on a 12% denaturing polyacrylamide gel.

To assay editing in vivo, total RNA was prepared from the S100 extract by extraction with Trizol^{TM} reagent (Invitrogen) as per the manufacturers instructions. The RNA was precipitated with isopropanol and treated with the restriction enzyme Cac8I (New England BioLabs, Ipswich, MA), followed by RQ1 DNase (Promega) to digest any remaining DNA. The RNA was extracted with phenol, precipitated with ethanol, and quantified. tRNA^{ala} was amplified by RT-PCR, using primers specific for the tRNA^{ala} sequence and the PCR product was sequenced (see below).

RT-PCR was used to measure amounts of the ADAT1 and hADAR2 mRNAs expressed in the *ipk1*Δ strains relative to those messages produced in the wild-type strain. Total RNA was prepared as described above, except after RQ1 DNase treatment, the restriction digest step was omitted and the RNA was further purified using an RNeasy^{TM} kit (Qiagen, Valencia, CA) according to the manufacturers instructions. The RNA was

reverse transcribed with Superscript™ II reverse transcriptase (Invitrogen, Carlsbad, CA) using an oligo-dT primer. A region of the cDNA (947-1175 of the ADAT1 gene, 2050-2324 of hADAR2 gene) was amplified by quantitative real-time PCR using a Roche Light Cycler with SYBR-Green fluorescent NTPs and gene specific primers. RT-PCR product amounts were normalized to that of a housekeeping gene (GAPDH) for quantitation.

Editing assays

hADAR2 concentrations in extracts prepared from BCY123 or BCY-*ipk1*Δ were quantified by western blotting. The blot was probed with a penta-His primary antibody (Qiagen) and alkaline phosphatase conjugated anti-mouse secondary antibody (Sigma-Aldrich, St. Louis, MO). Protein bands were detected using a fluorescent alkaline phosphatase ECF substrate (Amersham, Piscataway, NJ). The blot was scanned on a PhosphorImager, and the hADAR2 bands were quantified after generating a standard concentration curve of known amounts of a purified protein (the histidine tagged R_2D truncation of hADAR2, *S1*). Editing of the R/G site RNA by hADAR2 in vitro was performed as previously described (*S1*). Briefly, 5 nM RNA was reacted with increasing concentrations of hADAR2 present in yeast extracts (final concentrations of hADAR2 are indicated in Fig. 4A) for 1 hour at 30°C.

Yeast extracts for editing tRNA in vitro were prepared as described above and quantified by Bradford assay. 5 nM of A34 or A37 labeled $tRNA^{ala}$ was reacted with 10^{-3}, 10^{-2}, 0.1, 2.9, 5.8 μg/μl total protein for 1 hour at 30°C. IP_6 or IS_6 (concentrations noted in the legend to Fig. 4A; Sigma-Aldrich) were incubated with 0.1 μg/μl extract for

15 min at 30°C before adding 5 nM A37 labeled $tRNA^{ala}$. Reactions were completed as described above.

To observe editing in vivo, total RNA was prepared from the yeast S100 extracts (see above) and the tRNA was amplified by RT-PCR using gene specific primers. The PCR product was sequenced using a ^{32}P-labeled primer that hybridized to the non-template strand, and the Sequenase™ PCR product sequencing kit (USB, Cleveland, OH.) according to the manufacturers instructions. The sequencing products were separated on an 8% denaturing polyacrylamide gel. The gel was dried and exposed to a PhosphorImager plate overnight.

Supporting Figures

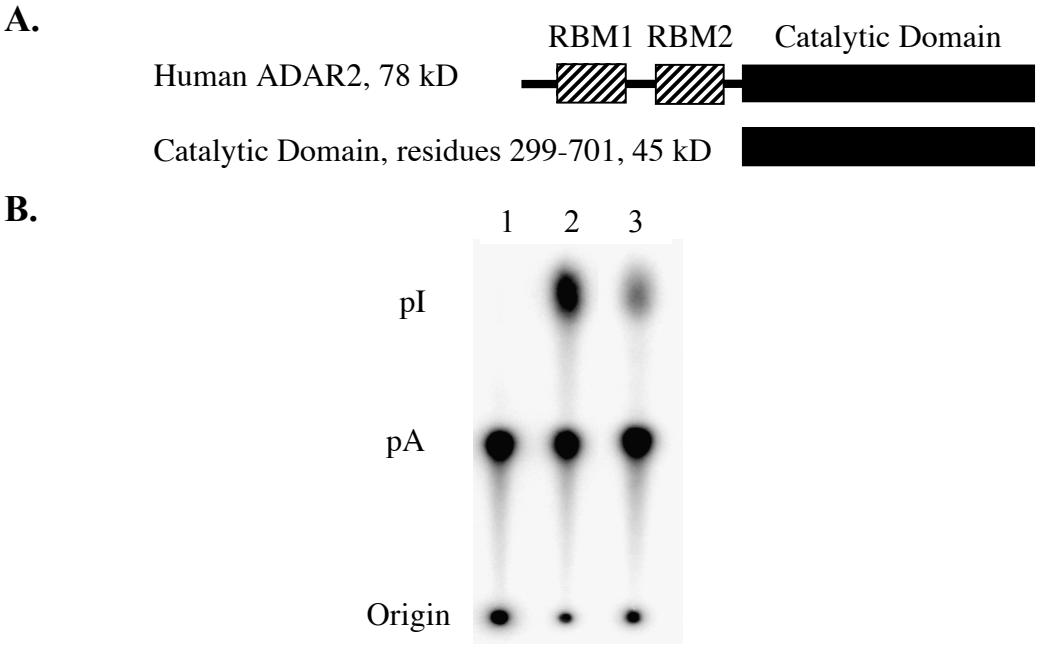

Figure S1. (A) Domain structure of hADAR2 and the catalytic domain construct used in this study. Striped rectangles, dsRBMs; filled rectangle, catalytic domain. **(B)** *In vitro* deamination assay. 10 nM ^{32}P-A-labeled dsRNA was incubated with 100 nM of full-

length hADAR2 or hADAR2-D for 1 hour. Reacted dsRNA was treated with P1 nuclease, the resulting 5'-NMPs separated by thin-layer chromatography, and the plate exposed to a phosphorimage screen. Lane 1, no protein control; Lane 2, hADAR2 treated dsRNA; Lane 3, hADAR2-D treated RNA. Origin, 5'AMP and 5'IMP spots are indicated.

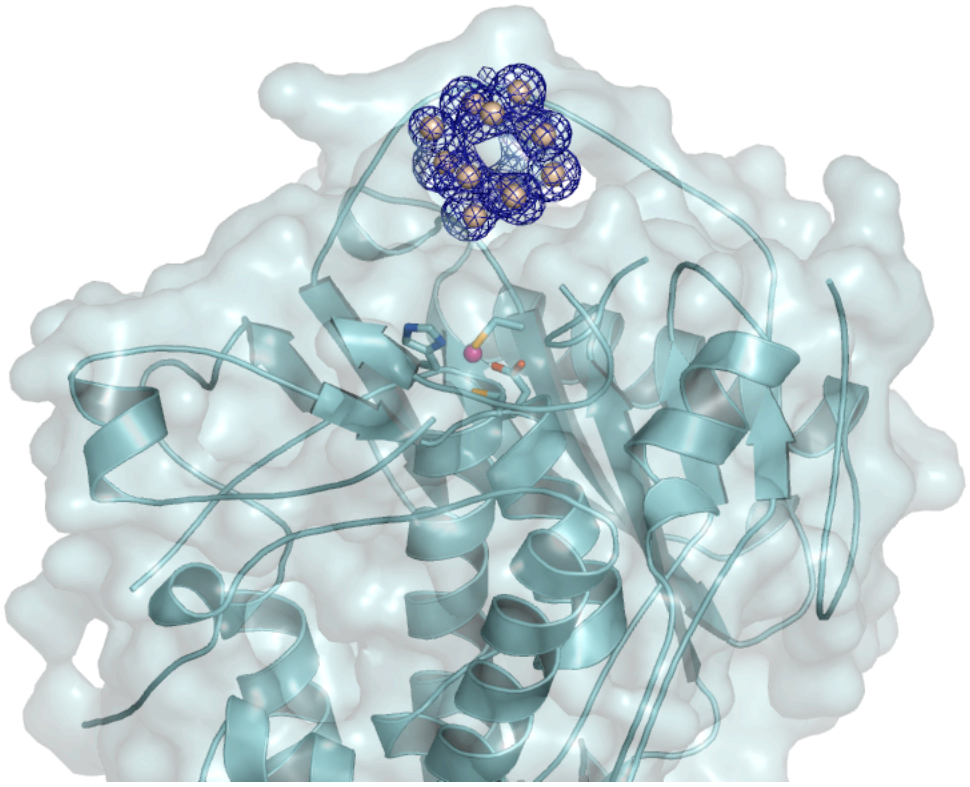

Figure S2. The electron density of a tungstate cluster containing 12 tungsten atoms observed in the heavy atom derivative (the tungsten atoms are modeled as grey spheres). The cluster is bound to a positively charged region on the surface near the active site of hADAR2-D (8 Å from the zinc, pink sphere). The density was calculated using ($F_{tungstate}$-F_{native}) with protein phases computed from the thimerosal derivative, and is contoured at 4σ.

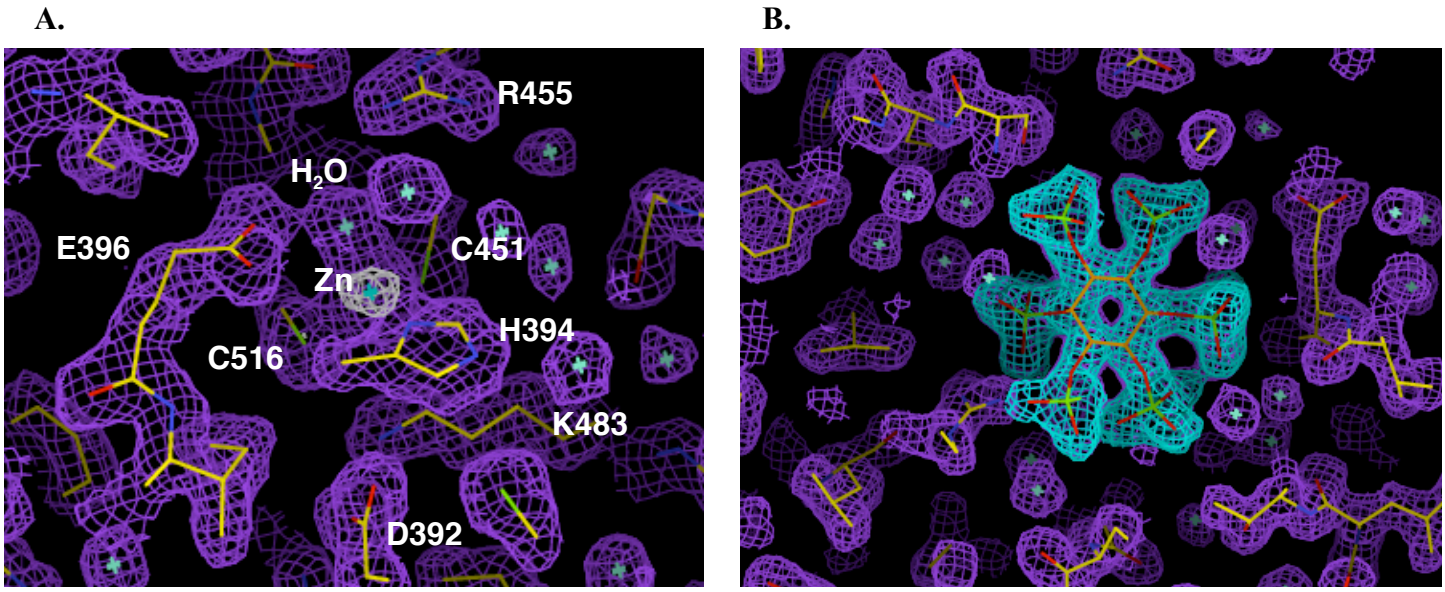

Figure S3. (A) $2F_{obs}$-F_{calc} electron density map (contoured at 1σ, purple or 9σ, white) of the region surrounding the active site Zn. **(B)** $2F_{obs}$-F_{calc} electron density map (purple) contoured at 1σ and F_{obs}-F_{calc} electron density map contoured at 3σ (cyan) calculated prior to inclusion of IP_6 in the model.

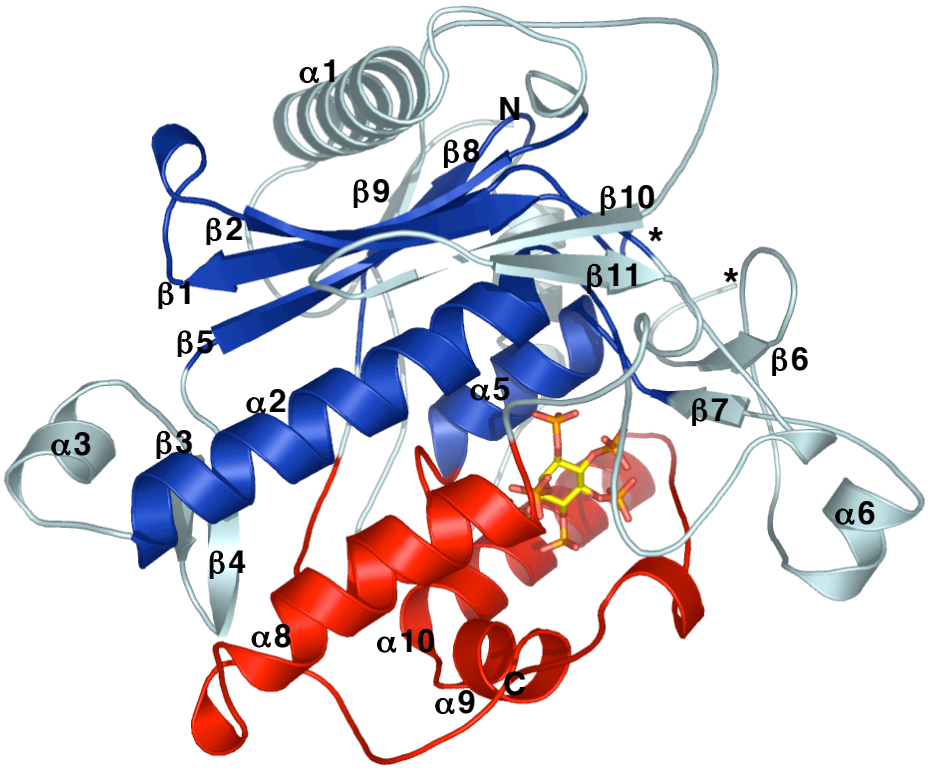

Figure S4. Another view of the ribbon model of hADAR2-D. The protein is rotated 90° about the vertical axis from Fig. 1B of the main text. IP_6 is shown as sticks. The active site zinc atom is obscured by β11. The color scheme is the same as Figure 1B of the main text. Ends of the disordered segment (residues 462-473) are indicated with asterisks (the beginning of the disordered region is obcured by β10).

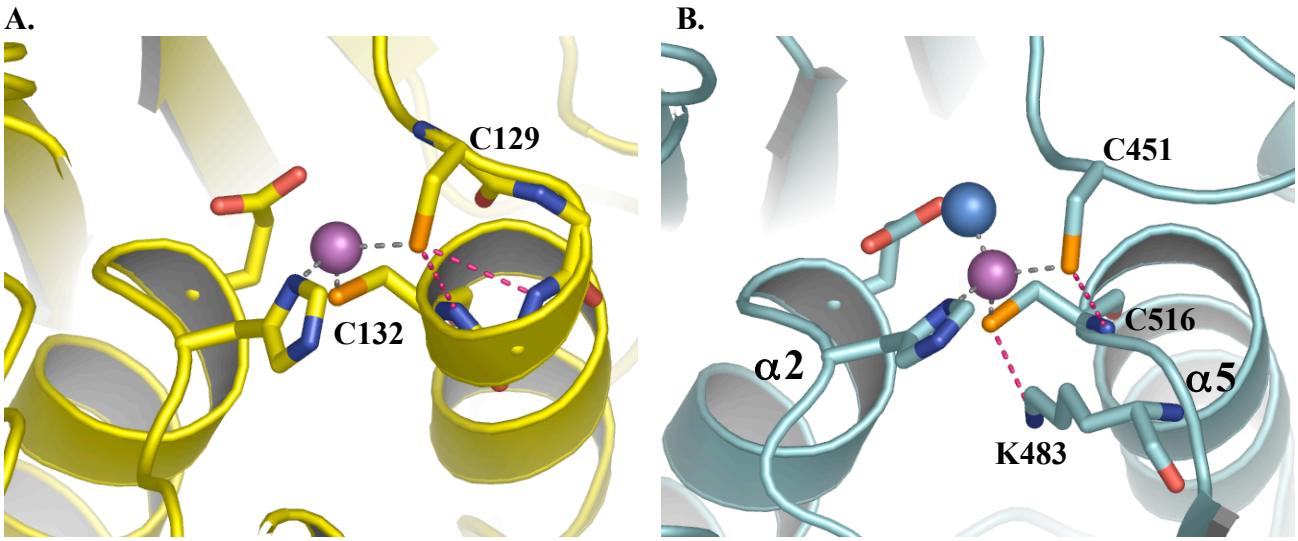

Figure S5. **(A)** The zinc coordinating environment of cytidine deaminase (*S15*). Zinc ion (magenta sphere), nucleophilic water (blue sphere), zinc coordinating bonds (grey dashed lines), hydrogen bonds (pink dashed lines). The thiolate of C129 forms hydrogen bonds with the backbone NH groups of residues H131 and C132 located at the N-terminus of the helix. These interactions are expected to reduce the negative character of the C129 thiolate, and thus increase the positive potential of the zinc ion. This may modulate catalysis by lowering the pKa of the coordinated water molecule that attacks the substrate C4 center of cytidine (*S16*). C132 is not within hydrogen bonding distance to any other residues. (**B)** The zinc-coordinating environment of hADAR2. A 64-residue loop separates C451 from C516, and the N-terminus of helix α5 is therefore less extended than in cytidine deaminase. The thiolate of C451 only forms one hydrogen bond with an amide NH (of C516). A consequent increase in water molecule pKa may be offset by a hydrogen-bonding interaction seen between the thiolate of C516 and the side chain of K483. The equivalent C132 of cytidine deaminase does not participate in hydrogen bonding interactions, whereas K483 is invariant in ADARs.

Table S1. Crystallographic Data

	Native	Thimerosal	Mercury Acetate	Sodium Tungstate
a (Å)	52.2	52.3	52.6	52.1
b (Å)	121.4	121.7	121.8	120.8
c (Å)	127.5	127.6	127.8	127.4
Resolution (Å)	20-1.7 (1.76-1.7)	20-2.7 (2.8-2.7)	20-2.7 (2.8-2.7)	20-2.6 (2.69-2.6)
# total reflections	388,243	228,747	54,141	120,441
# unique reflections	82,849	22,696	20,785	25,089
Completeness (%)	92.3 (62.5)	100 (100)	89.7 (87.9)	99.5 (99.8)
Mosaicity (˚)	0.5	0.6	0.7	0.7
I/σ(I)	35.2 (5.0)	21.2 (9.3)	10.9 (4.6)	8.7 (2.9)
R_{merge} [a]	3.9 (25.9)	13.4 (26.9)	9.2 (19.4)	11.2 (26.8)

Numbers in parenthesis are for the high-resolution bin

[a] $R_{merge} = 100x\Sigma|I-<I>|/\Sigma I$

Table S2. Refinement statistics

R_{cryst} (%) [a]	17.4
R_{free} (%) [b]	20.7
# Protein residues modeled	741
# Solvent molecules	670
RMSD bonds (Å)	0.015
RMSD angles (˚)	1.554
ϕ, ψ Most favored (%)	92.7
ϕ, ψ Additional Allowed (%)	6.4
<B> Overall (Å^2)	19.9
<B> Main Chain (Å^2)	17.8
<B> Side Chains (Å^2)	20.2
<B> Water (Å^2)	28.0
<B> IP_6 (Å^2)	14.6

[a] $R_{cryst} = 100x\Sigma||F_{obs}|-k|F_{calc}||/\Sigma|F_{obs}|$

[b] R_{free} = The R_{factor} against 5% of the data removed prior to refinement

Stereochemistry was analyzed using PROCHECK (*S17*)

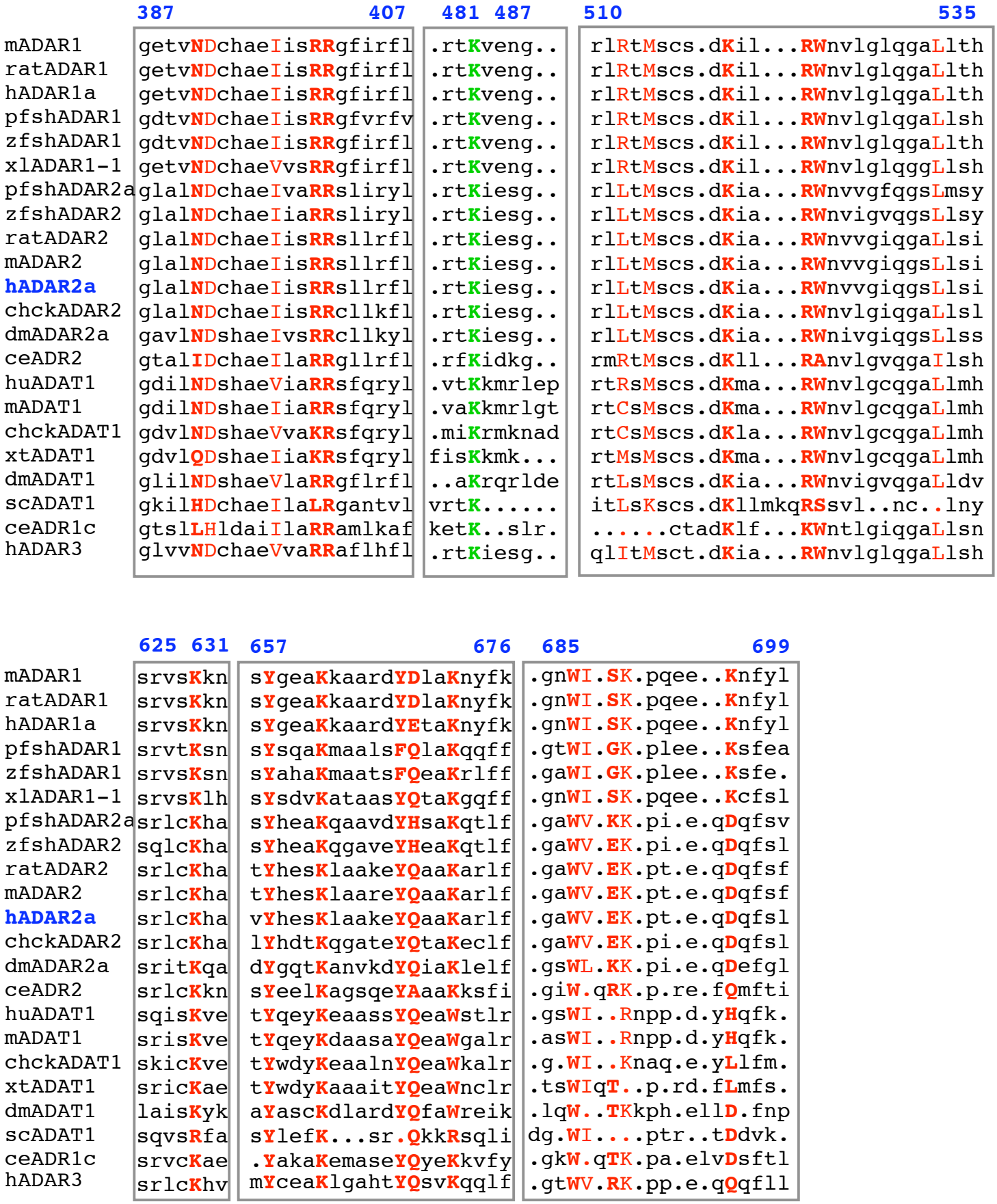
387 407 481 487 510 535
mADAR1 getvNDchaeIisRRgfirfl .rtKveng.. rlRtMscs.dKil...RWnvlglqgaLlth
ratADAR1 getvNDchaeIisRRgfirfl .rtKveng.. rlRtMscs.dKil...RWnvlglqgaLlth
hADAR1a getvNDchaeIisRRgfirfl .rtKveng.. rlRtMscs.dKil...RWnvlglqgaLlth
pfshADAR1 gdtvNDchaeIisRRgfvrfv .rtKveng.. rlRtMscs.dKil...RWnvlglqgaLlsh
zfshADAR1 gdtvNDchaeIisRRgfirfl .rtKveng.. rlRtMscs.dKil...RWnvlglqgaLlth
xlADAR1-1 getvNDchaeVvsRRgfirfl .rtKveng.. rlRtMscs.dKil...RWnvlglqggLlsh
pfshADAR2a glalNDchaeIvaRRsliryl .rtKiesg.. rlLtMscs.dKia...RWnvvgfqgsLmsy
zfshADAR2 glalNDchaeIiaRRsliryl .rtKiesg.. rlLtMscs.dKia...RWnvigvqgsLlsy
ratADAR2 glalNDchaeIisRRsllrfl .rtKiesg.. rlLtMscs.dKia...RWnvvgiqgaLlsi
mADAR2 glalNDchaeIisRRsllrfl .rtKiesg.. rlLtMscs.dKia...RWnvvgiqgsLlsi
hADAR2a glalNDchaeIisRRsllrfl .rtKiesg.. rlLtMscs.dKia...RWnvvgiqgsLlsi
chckADAR2 glalNDchaeIisRRcllkfl .rtKiesg.. rlLtMscs.dKia...RWnvlgiqgaLlsl
dmADAR2a gavlNDshaeIvsRRcllkyl .rtKiesg.. rlLtMscs.dKia...RWnivgiqgsLlss
ceADR2 gtalIDchaeIlaRRgllrfl .rfKidkg.. rmRtMscs.dKll...RAnvlgvqgaIlsh
huADAT1 gdilNDshaeViaRRsfqryl .vtKkmrlep rtRsMscs.dKma...RWnvlgcqgaLlmh
mADAT1 gdilNDshaeIiaRRsfqryl .vaKkmrlgt rtCsMscs.dKma...RWnvlgcqgaLlmh
chckADAT1 gdvlNDshaeVvaKRsfqryl .miKrmknad rtCsMscs.dKla...RWnvlgcqgaLlmh
xtADAT1 gdvlQDshaeIiaKRsfqryl fisKkmk... rtMsMscs.dKma...RWnvlgcqgaLlmh
dmADAT1 glilNDshaeVlaRRgflrfl ..aKrqrlde rtLsMscs.dKia...RWnvigvqgaLldv
scADAT1 gkilHDchaeIlaLRgantvl vrtK..... itLsKscs.dKllmkqRSsvl..nc..lny
ceADR1c gtslLHldaiIlaRRamlkaf ketK..slr. .....ctadKlf...KWntlgiqgaLlsn
hADAR3 glvvNDchaeVvaRRaflhfl .rtKiesg.. qlItMsct.dKia...RWnvlglqgaLlsh
625 631 657 676 685 699
mADAR1 srvsKkn sYgeaKkaardYDlaKnyfk .gnWI.SK.pqee..Knfyl
ratADAR1 srvsKkn sYgeaKkaardYDlaKnyfk .gnWI.SK.pqee..Knfyl
hADAR1a srvsKkn sYgeaKkaardYEtaKnyfk .gnWI.SK.pqee..Knfyl
pfshADAR1 srvtKsn sYsqaKmaalsFQlaKqqff .gtWI.GK.plee..Ksfea
zfshADAR1 srvsKsn sYahaKmaatsFQeaKrlff .gaWI.GK.plee..Ksfe.
xlADAR1-1 srvsKlh sYsdvKataasYQtaKgqff .gnWI.SK.pqee..Kcfsl
pfshADAR2a srlcKha sYheaKqaavdYHsaKqtlf .gaWV.KK.pi.e.qDqfsv
zfshADAR2 sqlcKha sYheaKqgaveYHeaKqtlf .gaWV.EK.pi.e.qDqfsl
ratADAR2 srlcKha tYhesKlaakeYQaaKarlf .gaWV.EK.pt.e.qDqfsf
mADAR2 srlcKha tYhesKlaareYQaaKarlf .gaWV.EK.pt.e.qDqfsf
hADAR2a srlcKha vYhesKlaakeYQaaKarlf .gaWV.EK.pt.e.qDqfsl
chckADAR2 srlcKha lYhdtKqgateYQtaKeclf .gaWV.EK.pi.e.qDqfsl
dmADAR2a sritKqa dYgqtKanvkdYQiaKlelf .gsWL.KK.pi.e.qDefgl
ceADR2 srlcKkn sYeelKagsqeYAaaKksfi .giW.qRK.p.re.fQmfti
huADAT1 sqisKve tYqeyKeaassYQeaWstlr .gsWI..Rnpp.d.yHqfk.
mADAT1 srisKve tYqeyKdaasaYQeaWgalr .asWI..Rnpp.d.yHqfk.
chckADAT1 skicKve tYwdyKeaalnYQeaWkalr .g.WI..Knaq.e.yLlfm.
xtADAT1 sricKae tYwdyKaaaitYQeaWnclr .tsWIqT..p.rd.fLmfs.
dmADAT1 laisKyk aYascKdlardYQfaWreik .lqW..TKkph.ellD.fnp
scADAT1 sqvsRfa sYlefK...sr.QkkRsqli dg.WI...ptr..tDdvk.
ceADR1c srvcKae .YakaKemaseYQyeKkvfy .gkW.qTK.pa.elvDsftl
hADAR3 srlcKhv mYceaKlgahtYQsvKqqlf .gtWV.RK.pp.e.qQqfll

Figure S6. Alignments for regions surrounding the residues that coordinate IP_6 in hADAR2 are shown, with hADAR2 numbering indicated in blue. IP_6 coordinating residues for backbone interactions (red capitals) and side chain interactions (bold, red capitals) are indicated. The alignment was prepared with the entire catalytic domain as input, using GCG software (Wisconsin Package Version 10.3, Accelrys Inc., San Diego, CA). Pileup, using default parameters, was used to align the following sequences (accession number; amino acids aligned, start-end): ADAR1, human (NM_001111; 833-1226), mouse (AF052506; 756-1152), rat (U18942; 779-1175), Xenopus laevis (U88065; 879-1270), pufferfish (AAF69764; 790-1194), zebrafish (NM_131596; 952-1382); ADAR2, human (NM_001112; 317-701), rat (NP_037026; 317-711), mouse (AF403106; 317-701), chicken (AF403119; 318-701), pufferfish (AF533143; 309-694), zebrafish (AF403113; 305-689), *D. melanogaster* (AF208535; 252-632), *C. elegans* (AF051275; 113-495); the entire open-reading frame for ADAT1, human (AF125188), mouse (NM_013925), chicken (NM_001012779), *Xenopus tropicalis* (CR762003), *D. melanogaster* (AF192530). This multiple sequence alignment was used as input to the program HmmerBuild to create a profile hidden Markov model (HMM) of the consensus (global alignment setting). The HMM file was then used with the program HmmerAlign to add the following to the alignment *S. cerevisiae* ADAT1, (AJ007297; 11-401), *C. elegans adr-1c* (AY150815; 617-964) and human ADAR3 (AF034837; 355-739). The alignment was optimized by selective manual manipulation using the program Seaview (*S18*). Manual manipulation was guided by alignments of the subgroups alone. Sequences diverge considerably in the region surrounding K483; the alignment shown was chosen because the conserved lysine of various subfamilies is aligned with K483 of hADAR2.

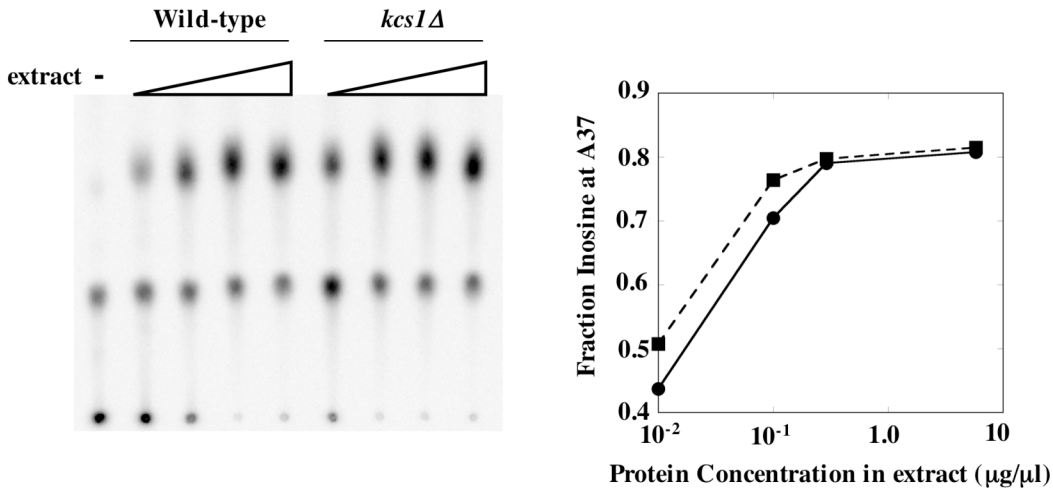

Figure S7. To rule out an ADAT1 requirement for IP_7, which is downstream of IP_6 in the inositol polyphosphate synthesis pathway, we assayed editing of A37 of $tRNA^{ala}$ by ADAT1 in extracts prepared from yeast unable to produce IP_7. The *KCS1* gene product phosphorylates IP_6 to form IP_7. ADAT1 from a *kcs1*Δ strain edits A37 with equal efficiency as ADAT1 from a wild-type strain, suggesting, along with the data from the *ipk1Δ* strain, that IP_6 is the required factor for editing activity. Left panel, TLC assay of tRNAala-A37 editing by ADAT1 in wild-type extracts or *kcs1*Δ extracts. Right panel, quantitation of inosine product as a function of wild-type or *kcs1*Δ extract concentration. Dashed line, ADAT1 activity in *kcs1*Δ extract; solid line, activity in wild-type extract.

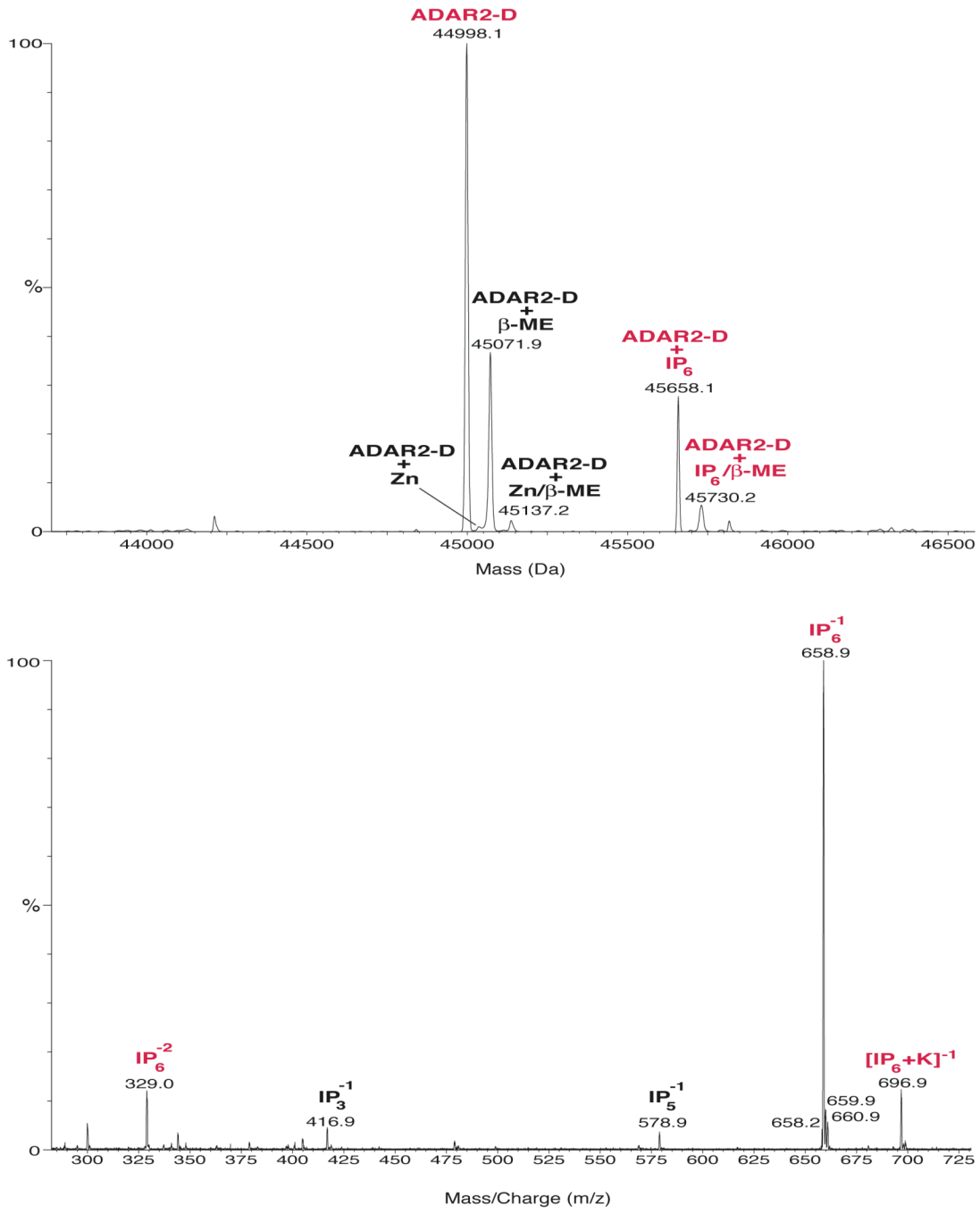

Figure S8. Electrospray mass spectrometry analysis of ADAR2-D and IP_6. Upper panel, molecular mass spectrum of native ADAR2-D. The sample was purified as described above, except Triton X-100 was not included in the lysis buffer. After purification, the protein was dialyzed against water and any remaining buffer was exchanged with water

using a Micron-10 centrifugal concentrator (Millipore, Billerica, MA). 5% acetonitrile (final concentration) was added to the sample before (+) ion electrospray data were collected in the 600-1400 m/z mass range. The spray voltage was 2.8 kV and cone voltage was 40 eV. The data were processed into a "molecular mass spectrum" using MAXENT software (Micromass, Beverly, MA). The ADAR2-D (44998.1 Da, observed; 44997.1 Da, calculated) peak and ADAR2-D peaks containing IP_6 (660 Da MW, i.e. neutral molecule) are labeled red. The 45071.9 Da and 45730.2 Da peaks are likely an oxidized cysteine/β-mecaptoethanol (β-ME) derivative (in the crystal structure, the thiol group of C634 exists in 2 conformations on the protein surface, and appears to be oxidized). In addition, the 45137.2 peak may contain zinc (65.4 Da). Lower panel, mass spectrum of inositol hexakisphosphate (dipotassium salt) purchased from Sigma (St. Louis, MO). The compound was dissolved in water (final concentration 10 mM) diluted with acetonitrile and triethylamine (final concentrations 50% and 3%, respectively) and analyzed by electrospray in (-) ion mode. The peaks corresponding to the -1 and -2 charge states as well as a potassium salt of IP_6 are labeled red. IP_3 and IP_5 contaminants/hydrolysis products are also labeled.

Supporting References

S1. M. R. Macbeth, A. T. Lingam, B. L. Bass, *RNA* **10**, 1563 (2004).
S2. B. L. Bass, H. Weintraub, *Cell* **48**, 607 (1987).
S3. Z. Otwinowski, in *Data Collection and Processing* L. Sawyer, Isaacs,N., and Bailey,S., Ed. (SERC Daresbury Laboratory, Warrington, UK, 1993) pp. 56-62.
S4. CCP4, *Acta Cryst.* **D50**, 760 (1994).
S5. T. C. Terwilliger, J. Berendzen, *Acta Crystallogr D Biol Crystallogr* **55**, 849 (1999).
S6. T. C. Terwilliger, *Acta Cryst.* **D56**, 965 (2000).
S7. D. E. McRee, *J. Struct. Biol.* **125**, 156 (1999).
S8. G. N. Murshudov, A. A. Vagin, E. J. Dodson, *Acta Crystallogr D Biol Crystallogr* **53**, 240 (1997).
S9. W. L. DeLano, *DeLano Scientific Inc.* **http://www.pymol.org** (2002).
S10. A. C. Wallace, R. A. Laskowski, J. M. Thornton, *Protein Eng.* **8**, 127 (1995).
S11. A. Wach, A. Brachat, R. Pohlmann, P. Philippsen, *Yeast* **10**, 1793 (1994).
S12. E. A. Winzeler *et al.*, *Science* **285**, 901 (1999).
S13. M. J. Moore, P. A. Sharp, *Science* **256**, 992 (1992).
S14. O. M. Stephens, H. Y. Yi-Brunozzi, P. A. Beal, *Biochemistry* **39**, 12243 (2000).
S15. L. Betts, S. Xiang, S. A. Short, R. Wolfenden, C. W. Carter, Jr., *J. Mol. Biol.* **235**, 635 (1994).
S16. D. C. Carlow, C. W. Carter, Jr., N. Mejlhede, J. Neuhard, R. Wolfenden, *Biochemistry* **38**, 12258 (1999).
S17. R. A. Laskowski, J. A. C. Rullmann, M. W. MacArthur, R. Kaptein, J. M. Thornton, *J. Appl. Cryst.* **26**, 283 (1993).
S18. N. Galtier, M. Gouy, C. Gautier, *Comput. Appl. Biosci.* **12**, 543 (1996).